

Mathematical Modelling of Fluid Flow in Open Circular Channels in Sewerage Systems

Research Article

David Chepkonga*, Winnie Kulei, Collins Owuor

Department of Mathematics, Jomo Kenyatta University of Agriculture and Technology, 62000-00200, Nairobi, Kenya

Received 24 February 2024; accepted (in revised version) 06 March 2024

Abstract: Amidst the nationwide flooding triggered by the rainy season compounded by El Niño, this study endeavors to devise a sophisticated mathematical model geared towards enhancing the efficiency of open circular channels. Focusing on key parameters like depth, velocity, and pressure within the context of incompressible, Newtonian, and steady flow dynamics, we aim to meticulously analyze their interplay. By delving into the impact of depth on flow characteristics, the influence of pressure on velocity, and the modulation of Reynolds and Froude numbers on velocity, our investigation unveils crucial insights. Leveraging MATLAB, we meticulously derive numerical solutions and visually represent our findings through insightful graphs. Given the inherent non-linearity of the governing equations; the continuity and momentum equations of motion. We used the finite difference method for the resolution. This robust model holds promise for diverse applications spanning water supply, treatment facilities, and irrigation networks, offering a comprehensive tool for optimizing operational efficiency.

MSC: 35Qxx • 65Mxx

Keywords: Mathematical Modelling • Open Channels • Finite Difference

© 2024 The Author(s). This is an open access article under the CC BY-NC-ND license (<https://creativecommons.org/licenses/by-nc-nd/3.0/>).

1. Introduction

The long rains and the ongoing El Niño have caused severe floods in the northern and southern regions of the country. The crisis stems from unprecedented flooding after a recent region-wide recovery from severe drought. In Mombasa County, water flows from the highlands to the lowlands, causing the overflow of already existing channels, which in turn results in floods and excess water remaining stagnant. Moreover, even during average rainfall, some informal settlements remain vulnerable to flooding, further emphasizing the urgent need for channels to be designed that can efficiently handle stormwater to prevent urban flooding and redirect excess water to agricultural lands. To address this issue, robust measures for modeling efficient channels to provide a pathway for stormwater to be safely conveyed away from urban areas should be adapted.

The classification of a channel as open or closed is determined by the state of its top; an open channel has an uncovered top, while a closed channel, also known as a conduit, has a covered top. Rivers and streams are open channels, while pipes and tunnels are closed channels. Open channels can be constructed with different cross-sections, such as trapezoidal, rectangular, and circular.

Research in open channel flow is a widespread area of study, encompassing investigations into both natural channels

* Corresponding author.

E-mail address(es): chepkongadavid@gmail.com (David Chepkonga), kjwinnie82@gmail.com (Winnie Kulei), owuorcollins92@gmail.com (Collins Owuor).

such as rivers and human-made structure such as irrigation canals. In the realm of open-channel flows, gravity, viscosity and inertia are the primary forces in play, each contributing significantly to the dynamics. The exploration of open channels has been a topic of discourse for an extended period. The following are some of the previous studies that have been done.

[1] Did modeling of fluid flow in open channel with circular cross-section. They investigate the effects of the flow depth, the cross section area of flow, channel radius, slope of the channel, roughness coefficient and energy coefficient on the flow velocity as well as the depth at which flow velocity is maximum. The Saint Venant partial differential equations of continuity and momentum governing free surface flow in open channels are highly nonlinear and therefore do not have analytical solutions. The Finite Difference Approximation method was used to solve these equations because of its accuracy, stability and convergence. It was established that for a given flow area, the velocity of flow increases with increasing depth and that the velocity is maximum slightly below the free surface. Moreover, increase in the slope of the channel and energy coefficient leads to an increase in flow velocity whereas increase in roughness coefficient, flow depth, radius of the conduit and area of flow leads to a decrease in flow velocity.

[2] Investigated the heat and mass transfer characteristics of non-Newtonian fluids, particularly in the context of physiological fluids modeled as couples stress fluids. The study delved into the intricate dynamics of two-dimensional non-Newtonian flow, attributing it to the metachronal wave generated by the synchronized oscillation of cilia, fine hair-like structures affixed to opposing walls within a channel. Through the derivation of a closed-form solution for the nonlinear differential equations governing the system, facilitated by convective boundary conditions. The investigation revealed the profound impact of a strong magnetic field on the fluid velocity, which diminishes for the base fluid but accelerates with increased cilia length. The interplay of parameters such as the Brinkman number, influencing energy addition, and the Biot number, affecting temperature profiles, underscores the complexity of the phenomenon. Furthermore, the Hartmann number emerges as a crucial factor, dictating the expansion and resistance of boluses within the channel.

[3] Focused on designing a circular open canal for a pisciculture system, where control over velocity and water height is maintained through the inlet and outlet system, ensuring continuous flow. By maintaining constant water volume and velocity, the system provides fish with a conducive environment. Utilizing Computational Fluid Dynamics (CFD), the canal flow is simulated, extracting parameters through numerical solutions of the Navier-Stokes equations. Implementing the outlet along the water movement path minimizes adverse suction effects, while modifications to the inlet, including guide vanes, facilitate the continuous flow of clean water, reducing turbulence. This integrated approach ensures optimal canal performance and water quality for pisciculture operations.

[4] Analyzed the interaction between very-large-scale motions (VLSMs) and secondary currents (SCs) in open-channel flows over ridge-covered fully rough beds. Using long-duration experiments and stereoscopic particle image velocimetry, the researchers explored a range of ridge spacings. In the absence of ridges, the flow exhibited quasi-two-dimensional behavior with prominent VLSM spectral signatures. However, when ridges were introduced, two distinct SC cells formed between neighboring ridges, effectively suppressing VLSMs. This suggests that ridge-induced SCs either absorb the energy of VLSMs or dominate their formation. Additionally, velocity spectra uncovered a novel feature associated with the meandering of alternating low- and high-momentum flow regions linked to instantaneous SC manifestations. Further analyses, including two-point velocity correlations and proper orthogonal decomposition, supported this observation, hinting at the instability arising from inflection points in the spanwise distribution of streamwise velocity within SC cells. These findings offer valuable insights into bed friction dynamics in open channels, suggesting potential fluctuations in friction factors based on the presence or absence of SCs and VLSMs.

[5] Did "Experimental Analysis of Sediment Incipient Motion in Rigid Boundary Open Channels," and the researchers conducted experiments to investigate the initiation of sediment motion in open channels with rigid boundaries. They employed various methodologies, likely including controlled flow rates and sediment sizes, to observe the conditions under which sediment particles first begin to move. By analyzing the results, which likely involved measuring critical shear stress or flow velocities required for particle entrainment, the researchers aimed to provide insights into the fundamental mechanics of sediment transport in such channels, contributing to the understanding of erosion processes in natural and engineered environments.

[6] Studied the flow characteristics of sharp-crested side circular orifices in irrigation systems focusing on both free and submerged flow conditions. The research aimed to analyze these characteristics through both analytical and experimental methods and to establish relationships for the coefficient of discharge under these conditions. The computed discharges based on the developed relationships closely matched the observed values, with discrepancies within $\pm 5\%$ for free orifices and $\pm 10\%$ for submerged orifices. The study also found that the discharge through side orifices is particularly sensitive to the head above the center of the orifice. Additionally, the research identified various parameters influencing jet angles and proposed relationships to predict these angles under different flow conditions.

[7] Investigated the impact of vegetation patches on turbulent flow properties in marine ecosystems using numerical simulations. The research was conducted through computational fluid dynamics (CFD) with ANSYS FLUENT, focusing on how circular vegetation patches of varying densities affect flow velocity, discharge capacity, and energy fluxes. The study employs Reynolds averaged Navier-Stokes equations and a Reynolds stress model (RSM) to analyze turbulent flow features near emergent and submerged vegetation patches. Results show that increasing vegetation

density decreases flow velocity and turbulent characteristics, fostering stability in aquatic ecosystems by promoting sediment deposition and supporting vegetation growth.

[8] Investigated time-dependent ferrofluid flow in a square enclosure with an open circular pipe by considering a variable magnetic field from an external source. Water-based ferrofluid with Fe₃O₄ nanoparticles was used, incorporating magnetohydrodynamics (MHD) and ferrohydrodynamics (FHD). The Incompressible Smoothed Particles Hydrodynamics (ISPH) method was applied for solving equations. Parameters like Hartmann number, magnetic number, solid volume fraction, and heated part location on the inner pipe were studied. Increasing the Hartmann number from 0 to 30 reduced maximum stream function values by 74.3%, and placing the heated part at the bottom right of the inner pipe enhanced heat transfer compared to other configurations.

[9] Conducted direct numerical simulation of open-channel flow over a regular pattern of spheres, focusing on fully rough flow regime at specific Reynolds numbers. It extends previous research on transitionally rough flow and aims to compare results with experiments. Statistical analysis of the flow field in the roughness sublayer and logarithmic region reveals that flow behavior near the roughness elements is influenced by both Reynolds number effects and geometric features, while farther from the wall, traditional roughness concepts apply. The roughness function is computed, expected to depend on relative submergence. Flow-roughness interaction primarily occurs above the virtual origin of the velocity profile, with maximum form-induced velocity fluctuations at sphere crests.

[10] Investigated convective heat transfer and entropy generation in slip flow of non-Newtonian power-law fluids through microchannels. It focused on both parallel-plate and circular geometries under uniform heat flux conditions. Using analytical methods, the study solved governing equations for fully developed laminar flows, considering non-linear slip boundary conditions and viscous dissipation. The analysis yielded closed-form solutions for velocity profiles, temperature distributions, Nusselt number, entropy generation rate, and Bejan number, dependent on parameters such as slip coefficient, power-law index, and Brinkman number. Results showed that increasing slip coefficient enhances Nusselt number and reduces average entropy generation rate. The impact of slip coefficient on Bejan number is influenced by Brinkman number. Lower values of power-law index or Brinkman number improve microfluidic system performance. Parallel-plate microchannels generate more entropy compared to circular ones under the same conditions. Viscous dissipation significantly affects heat transfer and entropy generation, highlighting its importance in designing thermally efficient microfluidic devices using non-Newtonian fluids.

[11] Focused on accurately predicting shear stress distribution in open channels, crucial for stable erodible-bed channels and sediment transport studies. Despite its importance, there's limited research on using entropy methods for this purpose. This study employs Tsallis entropy to estimate shear stress in open channels, using mean and maximum shear stresses across the channel cross-section. Prediction uncertainty is calculated, and the distribution of prediction error is analyzed before and after data normalization. The results show satisfactory performance of the Tsallis entropy model, with 95% Confidence Bounds closely matching observed shear stress values.

[12] Provided a thorough review of open-channel hydraulics, including theories, equations, and practical applications. The author delves into various subjects, including flow resistance, energy equations, uniform flow, progressively variable flow, and unsteady flow, focusing on using the Saint Venant equations to analyze unsteady open-channel flow. Chaudhry discusses the problems caused by channel form, roughness, and irregularity and provides techniques for solving the momentum and the continuity equation.

[13] Gave a thorough understanding of open channel hydraulics' concepts, theories, and practical applications. They also reviewed computational approaches and cutting-edge techniques for modeling and assessing open channel flow.

[14] Conducted an investigation focusing on the numerical modeling of turbulent flow in curved channels with compound cross-sections. They developed a mathematical model based on a curved orthogonal coordinate system, employing various algebraic stress models to simulate secondarily spiraled currents. The study delved into the impact of alterations in cross-cutting and canal curvature configurations on secondary motion, exploring the relationship between secondary stream patterns and different driving forces.

[15] Conducted a research study focused on the hydraulics of open rectangular and triangular channel flows, aiming to discern the hydraulic efficiency between the two configurations. The application of the laws of conservation of mass and momentum led to the derivation of non-linear partial differential equations, which could not be solved using analytical methods. Consequently, they employed the finite difference method for solving these equations. The study emphasized the significance of velocity and flow depth in determining discharge, and various parameters affecting velocity were investigated.

The findings indicated that flow velocity increased with depth, reaching its maximum slightly below the free surface. Additionally, an increase in channel slope, energy coefficient, and top width resulted in higher flow velocities, while an increase in roughness coefficient had the opposite effect. Notably, the research concluded that, for a fixed flow depth and width, an open rectangular channel exhibited greater hydraulic efficiency compared to an open triangular channel.

The insights gained from this study hold practical implications for applications such as flood control, irrigation, and the design of channels, including considerations for house gutter construction.

[16] Did a study on incompressible flow in open channels. They investigated the lateral inflow in an open trapezoidal

channel. They used the finite difference numerical method to solve the continuity, momentum, and chezy equations. They made assumptions that the only forces affecting the flow are the gravitational forces and that the fluid is unsteady and Newtonian. From the study, it was observed that the velocity of the fluid increases with an increase in depth. Also, an increase in the cross-sectional area led to a decrease in the flowing field. He recommended that the fluid could be more realistic if a two-dimensional flow were considered.

[17] Reviewed numerical simulations of lateral inflows in river bends. Their review highlighted the importance of understanding lateral inflows in river bends, which are crucial in channel dynamics and sediment transport. The review synthesized various numerical simulation techniques to study secondary flows, providing valuable insights for researchers and engineers on river hydraulics. By incorporating the findings of [17] Understanding flow behavior and dynamics in open channels, including the effects of lateral inflow and secondary flows, can be further enhanced, aiding in the development of more accurate and comprehensive models for open channel hydraulics.

[18] Conducted a study on the effect of a difference in angle in two lateral inflow channels on the main channel's velocity. This study examined the flow from two lateral inflow channels in an artificial open rectangular channel of an incompressible Newtonian fluid. The flow was assumed to be one-dimensional and unsteady. They used finite difference method to find approximate solutions. The goal was to look at the impact of the angle of the lateral inflow channels on the main channel flow velocity. The summary of the angle effect shows that 90° does not affect the key channel's flow velocity. 72° and 60° increases but 45° increases the flow velocity.

[19], [20] Conducted an investigation focusing on a model of open channel fluid flow characterized by a trapezoidal cross-section with a segment base. The primary aim of this research was to assess the relevance of trapezoidal cross-sections with segment bases in the design of drainage systems, specifically considering constant and uniform open channel flow. The study employed the finite-difference approximation method to solve the Saint-Venant partial differential equations governing free surface flow.

They found that an increase in the cross-sectional area of flow led to a decrease in flow velocity. The study observed that an increase in the radius of the circle forming the segment contributed to a reduction in flow velocity. The findings also indicated that an increase in the depth of flow, channel radius, and cross-sectional area resulted in a corresponding decrease in fluid velocity. Moreover, an increase in the bed slope of the waterway was associated with an increase in flow velocity. [21] Analyzed water flow behavior in trapezoidal open channels using the Saint-Venant model and the finite difference method. The study focused on understanding the hydraulic characteristics and flow patterns in trapezoidal channels commonly used in engineering applications.

[22] Explored the application of finite difference schemes to the one-dimensional Saint-Venant equation for simulating weir overflow. Their study demonstrated the effectiveness of finite difference schemes in accurately simulating the flow behavior and characteristics of weir overflow. The combined findings of both studies provide valuable insights into using numerical methods, specifically the finite difference approach, in modeling and analyzing open channel flows, including trapezoidal channels and weir overflow scenarios.

[23], [24] This study presents the development of a depth-averaged two-dimensional numerical model using finite difference method (FDM) on a staggered grid, solving governing equations with the Marker and Cell method by Harlow and Welch (1965). Employing explicit FDM for solving, first-order temporal derivative approximation, and second-order central difference for space discretization, the model's time step adheres to the Courant–Friedrichs–Lewy (CFL) condition, contingent on grid spacing and velocity components in both x- and y-directions. The research bifurcates into two phases: firstly, establishing the depth-averaged 2D model for flow simulation, and secondly, devising a module for bed load transport computation to simulate river morphology in regions with steep slopes and torrents. Applied to an artificial channel and a flood event in the Asungjun River segment of South Korea's Yangyang Namdae River, the model demonstrates good agreement with observed data, affirming its efficacy.

2. Mathematical Model

The foundation for the Model is provided by the Saint-Venant equations, which govern flow behavior in open channels. The Model considers the impact depth, pressure, and other relevant parameters on flow characteristics. By developing this Model, it becomes possible to analyze and anticipate flow patterns, water levels, and velocities within the open circular channel.

3. Assumptions

1. The flow is two dimensional in cylindrical coordinates.
2. The flow is steady.
3. The fluid is considered incompressible.
4. The forces causing the flow are due to gravity alone.

5. The fluid is Newtonian.
6. The flow is purely radial.

4. Governing equations

The Saint-Venant equations, which reflect mass and momentum conservation, are the foundation for the governing equations for fluid flow in an open circular channel. The momentum equation connects changes in momentum to the forces operating on the fluid, which is gravity in our case. These Saint-Venant equations are given by:

Continuity Equation:

$$\frac{\partial \rho}{\partial t} + \vec{\nabla}(\rho \cdot \vec{q}) = 0 \quad (1)$$

where ρ is the density, \vec{q} is the velocity vector, $\vec{\nabla}$ is the dell operator, t is the time.

Since flow is incompressible, the density is assumed to be constant; hence, the equation reduces to:

$$\vec{\nabla} \cdot \vec{q} = 0 \quad (2)$$

The velocity field for a 3D flow is given by $\vec{q} = ui + vj + wk$ and the dell operator is given by

$$\vec{\nabla} = i \frac{\partial}{\partial x} + j \frac{\partial}{\partial y} + k \frac{\partial}{\partial z}$$

Thus

$$(i \frac{\partial}{\partial x} + j \frac{\partial}{\partial y} + k \frac{\partial}{\partial z}) \cdot (ui + vj + wk) = 0 \quad (3)$$

$$\frac{\partial u}{\partial x} + \frac{\partial v}{\partial y} + \frac{\partial w}{\partial z} = 0 \quad (4)$$

In cylindrical coordinates, equation (4) will become

$$\frac{1}{r} \frac{\partial}{\partial r}(r u_r) + \frac{1}{r} \frac{\partial}{\partial \theta}(u_\theta) + \frac{\partial}{\partial z}(u_z) = 0 \quad (5)$$

The flow is in two dimensional in the r and z direction, but u_z is negligible: thus, equation (5) becomes

$$\frac{1}{r} \frac{\partial}{\partial r}(r u_r) = 0 \quad (6)$$

Momentum Equation:

$$\frac{\partial \vec{q}}{\partial t} + (\vec{q} \cdot \vec{\nabla}) \vec{q} = -\frac{1}{\rho} \vec{\nabla} P + \nu \nabla^2 \vec{q} + \vec{F} \quad (7)$$

where $\frac{\partial \vec{q}}{\partial t}$ is the temporal acceleration, ν is the kinematic viscosity, P is the pressure force, ∇^2 is the Laplacian operator, \vec{F} is the Body force, $(\vec{q} \cdot \vec{\nabla}) \vec{q}$ is the local acceleration.

Since the flow is steady, the above equation reduces to

$$(\vec{q} \cdot \vec{\nabla}) \vec{q} = -\frac{1}{\rho} \vec{\nabla} P + \nu \nabla^2 \vec{q} + \vec{F} \quad (8)$$

Dividing equation (8) all through by ρ

$$\rho (\vec{q} \cdot \vec{\nabla}) \vec{q} = -\vec{\nabla} p + \mu \nabla^2 \vec{q} + \rho \vec{F}_b \quad (9)$$

But $\nu = \frac{\mu}{\rho}$.

For buoyancy-driven flow, the governing equation is as follows:

$$\rho (\vec{q} \cdot \vec{\nabla}) \vec{q} = -\vec{\nabla} p + \nu \nabla^2 \vec{q} - \rho g \hat{k} \quad (10)$$

where $\vec{F}_b = -g \hat{k}$ and \hat{k} is the unit vector

The x-momentum equation for a two dimensional flow becomes

$$\rho (u \frac{\partial u}{\partial x} + w \frac{\partial u}{\partial z}) = -\frac{\partial p}{\partial x} + \mu (\frac{\partial^2 u}{\partial x^2} + \frac{\partial^2 u}{\partial z^2}) + \rho g_x \quad (11)$$

The y-momentum becomes

$$\rho(u \frac{\partial w}{\partial x} + v \frac{\partial w}{\partial z}) = -\frac{\partial p}{\partial z} + \mu(\frac{\partial^2 w}{\partial x^2} + \frac{\partial^2 w}{\partial z^2}) + \rho g_z \tag{12}$$

In cylindrical coordinates, they become

r-component

$$\rho(u_r \frac{\partial u_r}{\partial r} + u_z \frac{\partial u_r}{\partial z} - \frac{u_\theta^2}{r}) = -\frac{\partial p}{\partial r} + \mu(\nabla^2 u_r - \frac{u_r}{r^2}) + \rho g_r \tag{13}$$

z-component

$$\rho(u_r \frac{\partial u_z}{\partial r} + u_z \frac{\partial u_z}{\partial z}) = -\frac{\partial p}{\partial z} + \mu(\nabla^2 u_z) + \rho g_z \tag{14}$$

Since the flow is purely radial and velocity in the z direction is negligible, the equation reduces to

r-component

$$\rho(u_r \frac{\partial u_r}{\partial r}) = -\frac{\partial p}{\partial r} + \mu \frac{1}{r} \frac{\partial}{\partial r} (r \frac{\partial u_r}{\partial r} - \frac{u_r}{r^2}) + \rho g_r \tag{15}$$

z-component

$$0 = -\frac{\partial p}{\partial z} + \rho g_z \tag{16}$$

5. Non-dimensionalization of the governing equations

This is the process of completely or partially eliminating physical dimensions using the appropriate variable substitution from an equation involving physical quantities. When using this technique, problems involving measured units can be made simpler and more parameterized. It can decrease the free parameters and facilitate the examination of the current issue. The non-dimensionalization equation facilitates a better understanding of the relative sizes of the different variables in the equation. This results in identifying small terms in the equation once the non-dimensionalization procedure appropriately chooses the scaler. The solution can be made simpler by disregarding the smaller terms in favor of the larger ones. By choosing distinctive dimensionless quantities, the governing equations are non-dimensionalized.

Let: $u_r^* = \frac{u_r}{U} \implies u_r = U u_r^*, r^* = \frac{r}{R} \implies r = r^* R$

$p^* = \frac{p}{p_o} \implies p = p_o p^*, z^* = \frac{z}{R} \implies z = R z^*$

Using the chain rule we obtain the first and the second order equation

$$\frac{\partial u_r}{\partial r} = \frac{\partial u_r}{\partial u_r^*} \cdot \frac{\partial u_r^*}{\partial r^*} \cdot \frac{\partial r^*}{\partial r} = \frac{U}{R} \cdot \frac{\partial u_r^*}{\partial r^*} \tag{17}$$

$$\frac{\partial p}{\partial r} = \frac{\partial p}{\partial p^*} \cdot \frac{\partial p^*}{\partial r} = \frac{p_o}{R} \cdot \frac{\partial p^*}{\partial r^*} \tag{18}$$

$$\frac{\partial p}{\partial z} = \frac{\partial p}{\partial p^*} \cdot \frac{\partial p^*}{\partial z^*} \cdot \frac{\partial z^*}{\partial z} = \frac{p_o}{R} \cdot \frac{\partial p^*}{\partial z^*} \tag{19}$$

$$\frac{\partial^2 u_r}{\partial r^2} = \frac{\partial}{\partial r} (\frac{\partial u_r}{\partial r}) = \frac{\partial}{\partial r} (\frac{U}{R} \cdot \frac{\partial u_r^*}{\partial r^*}) = \frac{U^2}{R^2} \cdot \frac{\partial^2 u_r^*}{\partial r^{*2}} \tag{20}$$

Substituting equation (15) in the continuity equation (16), the equation reduces to

$$\frac{U}{R} \frac{\partial u_r^*}{\partial r^*} = 0 \tag{21}$$

Substituting equations (17),(18),(19) and (20) in the r-momentum equation (15), the equation reduces to

$$\rho \frac{U^2}{R} u_r^* \frac{\partial u_r^*}{\partial r^*} = -\frac{p_o}{R} \frac{\partial p^*}{\partial r^*} + \frac{\mu U}{R^2 r^*} \frac{\partial u_r^*}{\partial r^*} + \frac{\mu U}{R^2} \frac{\partial^2 u_r^*}{\partial r^{*2}} - \frac{\mu U}{R^4 r^{*3}} \frac{\partial u_r^*}{\partial r^*} - \frac{2\mu U}{R^8 r^{*8}} u_r^* + \rho g_r \tag{22}$$

Multiplying by $\frac{R}{\rho U^2}$ we get

$$u_r^* \frac{\partial u_r^*}{\partial r^*} = -\frac{p_o}{\rho U^2} \frac{\partial p^*}{\partial r^*} + \frac{\mu}{\rho R U} \frac{\partial u_r^*}{\partial r^*} + \frac{\mu}{\rho R U} \frac{\partial^2 u_r^*}{\partial r^{*2}} - \frac{\mu}{\rho U R^3 r^{*3}} \frac{\partial u_r^*}{\partial r^*} - \frac{2\mu}{\rho R^7 U r^{*8}} u_r^* + \frac{R g_r}{U^2} \tag{23}$$

But Reynolds's and Froude's numbers are given by

$$Re = \frac{\rho U R}{\mu}, Fr = \frac{U}{\sqrt{g R}}$$

Equation (23) reduces to

$$u_r^* \frac{\partial u_r^*}{\partial r^*} = -\frac{p_o}{\rho U^2} \frac{\partial p^*}{\partial r^*} + \frac{1}{Re r^*} \frac{\partial u_r^*}{\partial r^*} + \frac{1}{Re} \frac{\partial^2 u_r^*}{\partial r^{*2}} - \frac{1}{Re R^2 r^{*3}} \frac{\partial u_r^*}{\partial r^*} - \frac{2}{Re R^6 r^{*8}} u_r^* + \frac{1}{Fr} \tag{24}$$

Substituting equation (3.19) in the z-momentum equation (3.16), the equation reduces to

$$0 = \frac{p_o}{R} \frac{\partial p^*}{\partial z^*} + \rho g_z \tag{25}$$

6. Boundary conditions

Boundary values are crucial in solving ordinary differential equations (ODEs) because they define the conditions at the boundaries of the domain over which the differential equation is defined. In many practical applications, the behavior of the system being modeled is influenced by conditions at its boundaries.

Here are a few reasons why boundary values are significant in solving ODEs:

- (i) **Physical Constraints:** Boundary values often represent physical constraints or conditions that must be satisfied by the solution. For example, in a heat conduction problem, the temperature at the boundaries of a material might be specified or the heat flux might be prescribed.
- (ii) **Uniqueness of Solution:** For many differential equations, specifying boundary conditions is necessary to ensure the existence and uniqueness of the solution. Without appropriate boundary conditions, there may be multiple solutions or no solution at all.
- (iii) **Determining Specific Solutions:** Boundary conditions help to determine specific solutions to the ODE. They provide additional information that narrows down the set of possible solutions to one that satisfies both the differential equation and the boundary conditions.
- (iv) **Physical Interpretation:** Boundary conditions often have a physical interpretation that helps to understand the behavior of the system being modeled. They can represent constraints imposed by the physical environment in which the system operates.

The boundary conditions for the study problem are:

at $r=0$

$$u_r = u_\infty, P = P_\infty$$

at $r = \infty$

$$u_r = u_w, P = P_w$$

7. Method of solution

7.1. Finite difference method

The finite difference approximations of these partial differential equations are obtained from Taylor's series expansion of the independent variables [25]. From definition

$$u_r = \frac{\partial u_r}{\partial r} = \lim_{\Delta r \rightarrow 0} \frac{u(r + \Delta r) - u(r)}{\Delta r} \quad (26)$$

The finite difference method offers a powerful approach for addressing problems with boundary or initial value conditions by discretizing the problem's domain into a grid or mesh. Through this discretization, derivatives in the original differential equation are approximated using finite difference approximations. The method employs discrete points to estimate the function's rate of change at each grid point, constructing an algebraic equation system by substituting these approximations into the original equation. Solving this system provides an approximation to the solution of the original differential equation [26]. Key considerations for employing this technique include defining the grid spacing, the number of grid points, and ensuring proper boundary or initial conditions, which alongside the order of the finite difference approximations [27], significantly impact the method's accuracy.

7.2. The forward finite difference method

In the forward finite difference method, the derivative is estimated by computing the difference between the function values at a given point and a slightly displaced point in the forward direction, divided by the displacement. The following substitutions are derived using this method:

$$\begin{aligned} \frac{\partial u_r^*}{\partial r^*} &= \frac{u_r^*{}_{(i+1,k)} - u_r^*{}_{(i,k)}}{\Delta r^*} \\ \frac{\partial p^*}{\partial r^*} &= \frac{p^*{}_{(i+1,k)} - p^*{}_{(i,k)}}{\Delta r^*} \\ \frac{\partial^2 u_r^*}{\partial r^{*2}} &= \frac{u_r^*{}_{(i+1,k)} - 2u_r^*{}_{(i,k)} + u_r^*{}_{(i-1,k)}}{(\Delta r^*)^2} \\ \frac{\partial p^*}{\partial z^*} &= \frac{p^*{}_{(i+1,k)} - p^*{}_{(i,k)}}{\Delta z} \end{aligned}$$

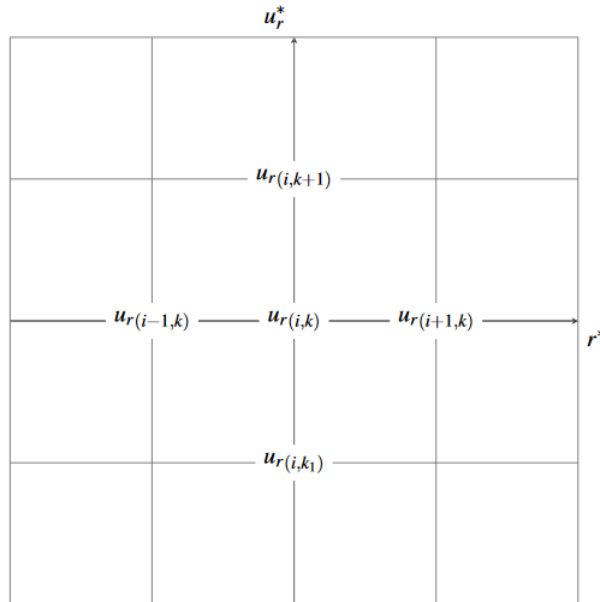


Fig. 1. Finite difference mesh

Replacing the above substitution in the governing equations

Continuity equation

$$\frac{U}{R} \frac{u_r^*(i+1,k) - u_r^*(i,k)}{\Delta r^*} = 0 \tag{27}$$

r-momentum

$$u_{r,i,k}^* \left(\frac{u_r^*(i+1,k) - u_r^*(i,k)}{\Delta r^*} \right) = - \frac{p_{o(i,k)}}{\rho(i,k)U^2} \left(\frac{p^*(i+1,k) - p^*(i,k)}{\Delta r^*} \right) + \frac{1}{Re r^*(i,k)} \left(\frac{u_r^*(i+1,k) - u_r^*(i,k)}{\Delta r^*} \right) + \frac{1}{Re} \left(\frac{u_r^*(i+1,k) - 2u_r^*(i,k) + u_r^*(i-1,k)}{(\Delta r^*)^2} \right) - \frac{1}{Re R^2 r^{*3}(i,k)} \left(\frac{u_r^*(i+1,k) - u_r^*(i,k)}{\Delta r^*} \right) - \frac{2}{Re R^6 r^{*8}(i,k)} u_{r,i,k}^* + \frac{1}{Fr} \tag{28}$$

z-momentum

$$0 = \frac{p_{o(i,k)}}{R} \left(\frac{p^*(i+1,k) - p^*(i,k)}{\Delta z} \right) + \rho g_z \tag{29}$$

Making $u_{r,i+1,k}^*$ the subject in equation (28) and $p_{i+,k}^*$ in equation (29) the equations become.

$$u_{r,i+1,j}^* = \frac{p_{o(i,j)}}{\rho(i,j)U^2} (p^*(i+1,j) - p^*(i,j)) - \frac{1}{Re} u_{r(i,j)}^* - \frac{1}{Re} \frac{2u_{r(i,j)}^*}{\Delta r^*} + \frac{1}{Re} \frac{u_{r(i-1,j)}^*}{\Delta r^*} + \frac{1}{Re R^2 r^{*3}(i,j)} u_{r(i,j)}^* - \frac{2\Delta r^*}{Re R^6 r^{*8}(i,j)} + \frac{\Delta r^*}{Fr} + u_{r(i,j)}^{*2} \div \left(u_{r,i+1,j}^* - \frac{1}{Re r^*(i,j)} - \frac{1}{Re \Delta r^*(i,j)} + \frac{1}{Re R^2 r^{*3}(i,j)} \right) \tag{30}$$

$$p^*(i+1,k) = \frac{R}{p_{o(i,k)}} p^*(i,k) - \frac{R}{p_{o(i,k)}} \Delta z \rho g_z \tag{31}$$

The FDM representation of the equation of momentum in the r and z direction is the governing equation that will be applied in this study.

8. Results and Discussions

MATLAB software was used to simulate the equations (30) and (31). The flow parameters of Reynold's and Froude's numbers were investigated to determine how they affect the velocity.

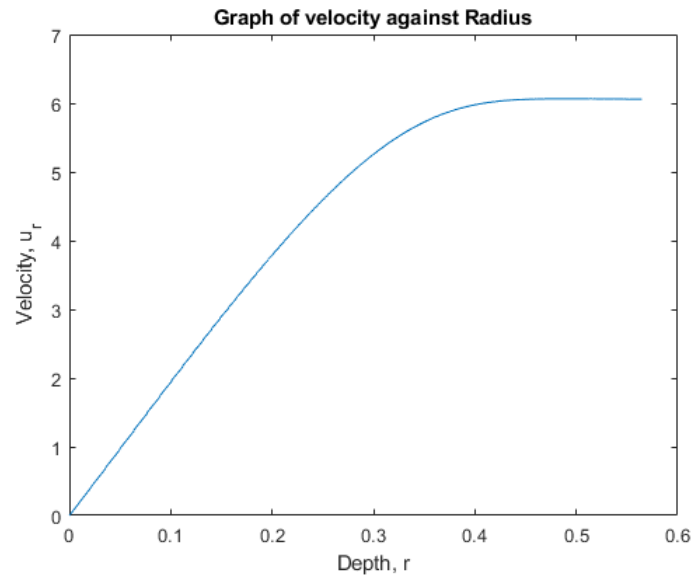


Fig. 2. Graph of velocity against radius

8.1. The velocity profiles of the flow

The results on velocity profiles indicates that, an increase in the radius leads to an increase in velocity. From the figure (2), it is observed velocity decreases with depth. The fluid flow velocity at the channel bottom is zero due to the non-slip condition of fluids. The non-slip condition states that a fluid in contact with a surface will achieve the same velocity as the surface. Since at the channel bottom, the surface is stationary, the flow velocity at this section of the channel will be zero. However, as you move vertically upwards, the velocity increases since the frictional forces decrease and velocity becomes maximum slightly below the free surface. At the free surface, the velocity is not maximum due to surface tension that is caused by strong cohesive forces between the fluid molecules.

8.2. The pressure profiles of the flow

From the figure (3), its observed that an increase in depth leads to an increase in pressure. The results indicate that an increase in the depth leads to an increase in the pressure.

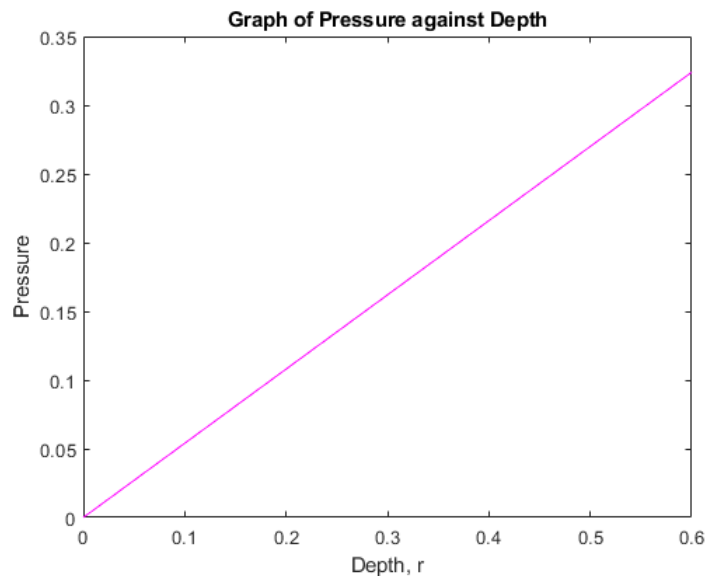


Fig. 3. Graph of pressure against radius

As depth increases within the circular channel, the pressure equation reveals a corresponding rise in pressure. This

phenomenon occurs because at greater depths, there is a larger volume of fluid above that particular point. Consequently, the increased weight of this additional fluid column exerts a greater force, resulting in elevated pressure levels.

8.3. The effects of pressure on the velocity profile

From the figure (4), the pressure decreases with increase in velocity. The observed trend indicates a negative correlation between fluid velocity and pressure within the system. Specifically, as fluid velocity increases, pressure tends to decrease, and conversely, as fluid velocity decreases, pressure tends to increase. This negative correlation suggests an inverse relationship between the two variables: as one variable increases, the other tends to decrease, and vice versa.

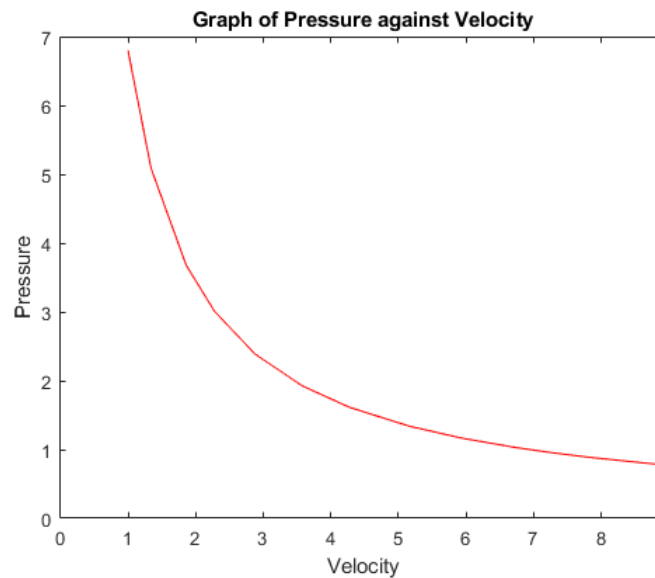


Fig. 4. Graph of pressure against velocity

According to Bernoulli's principle, as the velocity of a fluid increases, the pressure decreases, and vice versa. This relationship arises from the conservation of energy in a fluid flow system, where an increase in fluid velocity is accompanied by a decrease in pressure energy and vice versa. This principle is fundamental in fluid dynamics and is applicable in various contexts, including the flow of liquids and gases in pipes, channels, and around objects.

9. The effects of varying flow parameters on Flow variables

9.1. Effects of Reynolds number on the velocity Profiles

From the figure (5) the velocity profile increases with an increase in the Reynold's Number

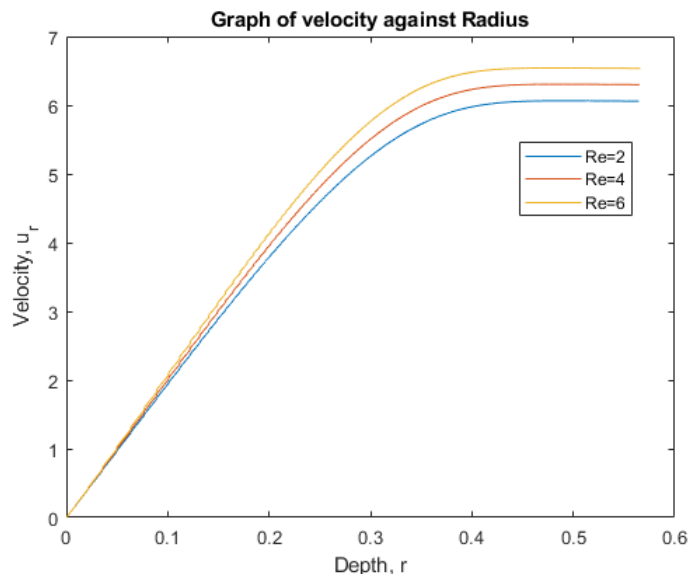


Fig. 5. Graph of velocity with varying Reynolds number

In the depicted graph illustrating the correlation between Reynolds number and flow velocity, a clear pattern emerges, reflecting the intricate balance between inertial and viscous forces in fluid dynamics. With increasing Reynolds numbers, indicating a greater dominance of inertial forces relative to viscous forces, there is a corresponding rise in flow velocity. Conversely, as Reynolds numbers decrease, signifying a shift towards viscous forces dominating over inertial forces, a decrease in flow velocity is observed. This dynamic interplay between Reynolds number and flow velocity underscores the fundamental principles governing fluid behavior, offering valuable insights into the nature of fluid flow phenomena.

9.2. Effects of Froude's number on the velocity Profiles

From figure (6) the velocity profile increases with an increase in the Froude's number

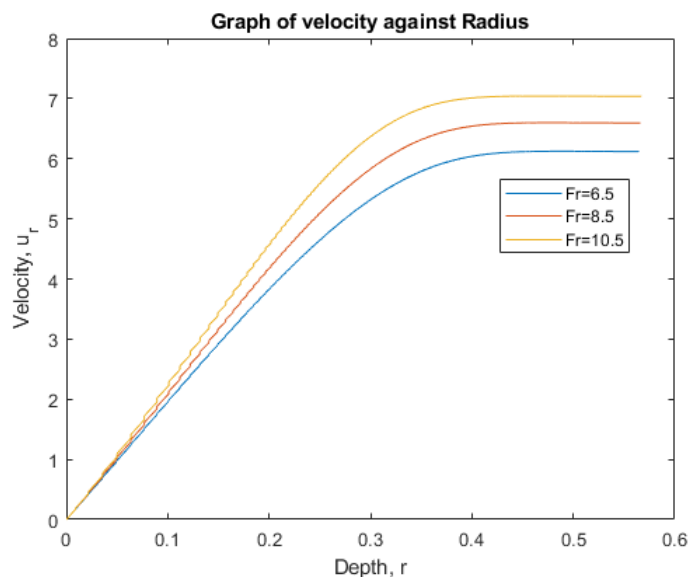


Fig. 6. Graph of velocity against radius with varying Froude's number

When the Froude number is high, it indicates a dominance of inertial forces over gravitational forces. Consequently, velocities tend to be high under such conditions. Conversely, when the Froude number is low, gravitational forces exert greater influence over inertial forces, resulting in lower velocities. This relationship highlights the critical role of the Froude number in characterizing the balance between inertial and gravitational forces within fluid systems, offering insights into the flow behavior and dynamics of various phenomena, such as open channel flows and wave propagation.

10. Validation of results

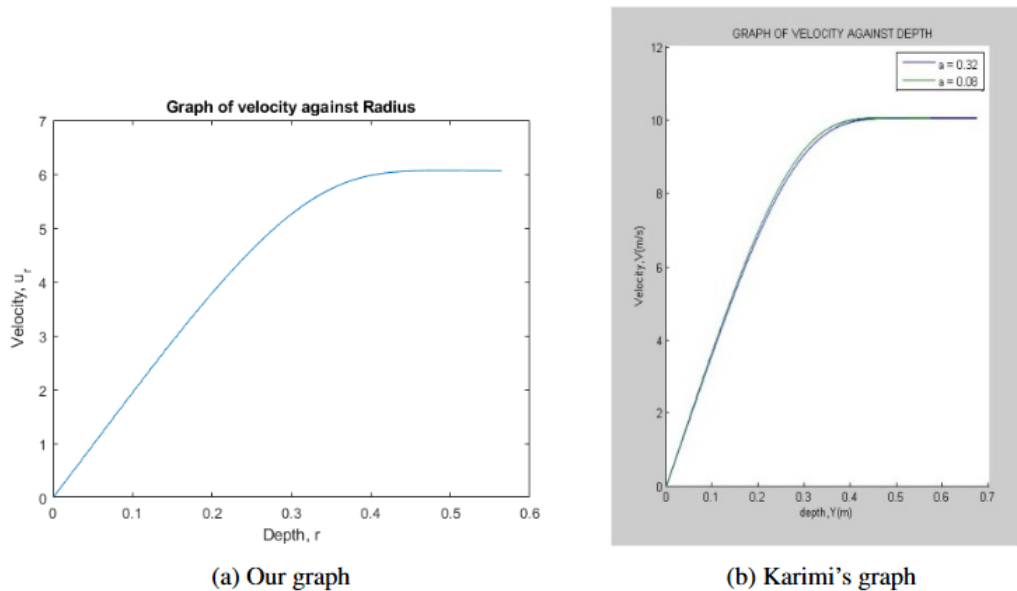


Fig. 7. Validation of results

Based on the velocity profiles observed, it's evident that an upward trend exists: as depth increases from the surface, velocity also increases. This finding aligns with the conclusions drawn by [16] as seen on figure (7), [28], who examined fluid flow in an open trapezoidal channel and similarly found that flow velocity correlates positively with depth.

Acknowledgements

The authors would like to thank Jomo Kenyatta University of Agriculture and Technology for the valuable support accorded during the research period.

References

- [1] M. Kinyanjui, D. Tsombe, J. Kwanza, and K. Gaterere, *Journal of Agriculture, Science and Technology* **13**, 78 (2011).
- [2] M. Nazeer, S. Saleem, F. Hussain, S. Iftikhar, and A. Al-Qahtani, *International Communications in Heat and Mass Transfer* **124**, 105274 (2021).
- [3] A. Jebelli, M. S. Zare, N. Lotfi, and M. C. Yagoub, *Water-Energy Nexus* **6**, 96 (2023).
- [4] A. Zampiron, S. Cameron, and V. Nikora, *Journal of Fluid Mechanics* **887**, A17 (2020).
- [5] M. J. S. Safari, H. Aksoy, N. E. Unal, and M. Mohammadi, *Environmental Fluid Mechanics* **17**, 1281 (2017).
- [6] A. Hussain, Z. Ahmad, and C. Ojha, *Flow Measurement and Instrumentation* **52**, 57 (2016).
- [7] H. Tariq, U. Ghani, N. Anjum, and G. A. Pasha, *Journal of Hydrology and Hydromechanics* **70**, 128 (2022).
- [8] A. M. Aly and S. E. Ahmed, *International Communications in Heat and Mass Transfer* **110**, 104412 (2020).
- [9] M. Mazzuoli and M. Uhlmann, *Journal of Fluid mechanics* **824**, 722 (2017).
- [10] M. Kiyasatfar, *International Journal of Thermal Sciences* **128**, 15 (2018).

- [11] A. Kazemian-Kale-Kale, H. Bonakdari, A. Gholami, Z. S. Khozani, A. A. Akhtari, and B. Gharabaghi, *Physica A: Statistical Mechanics and its Applications* **510**, 558 (2018).
- [12] M. H. Chaudhry, *Open-channel flow* (2020).
- [13] A. O. Akan and S. S. Iyer, *Open channel hydraulics* (Butterworth-Heinemann, 2021).
- [14] X. Shao, H. Wang, and Z. Chen, *Advances in water resources* **26**, 525 (2003).
- [15] J. W. Thiong'o, Ph.D. thesis (2013).
- [16] S. M. Karimi, Ph.D. thesis, JKUAT-PAUSTI (2018).
- [17] R. Shaheed, A. Mohammadian, and X. Yan, *Water* **13**, 884 (2021).
- [18] A. Chirchir, J. Kandie, and J. Maremwa, *The effect of a difference in angle in two lateral inflow channels on the main channel's velocity* (2021).
- [19] P. K. Marangu, E. K. Mwenda, and D. Theuri (2016).
- [20] K. V. Reddy and M. G. Reddy, *Int J Adv Appl Math Mech* **2**, 126 (2014).
- [21] G. Natasha, V. Noviantri, et al., *Procedia Computer Science* **157**, 6 (2019).
- [22] N. L. H. Zandrato, A. Chrysanti, B. P. Yakti, M. B. Adityawan, and Y. Suryadi, in *MATEC Web of Conferences* (EDP Sciences, 2018), vol. 147, p. 03011.
- [23] D. T. An and P. S. Deog, *Environmental Modeling & Assessment* **22**, 91 (2017).
- [24] K. Uchdadiya and J. Patel, *International Journal of Advances in Applied Mathematics and Mechanics* **2**, 88 (2014).
- [25] B. Pandita and V. Kulkarni, *International Journal of Advances in Applied Mathematics and Mechanics* **3**, 100 (2015).
- [26] D. Chepkonga, K. Roy, and G. Kangethe, *International Journal of Advances in Applied Mathematics and Mechanics* (2019).
- [27] P. G. Moakher, M. Abbasi, and M. Khaki, *International Journal of Advances in Applied Mathematics and Mechanics* **2**, 87 (2015).
- [28] V. Kaigalula, J. Okelo, S. Mutua, and O. Muvengei, *Journal of Applied Mathematics and Physics* **11**, 3287 (2023).

Submit your manuscript to IJAAMM and benefit from:

- ▶ Rigorous peer review
- ▶ Immediate publication on acceptance
- ▶ Open access: Articles freely available online
- ▶ High visibility within the field
- ▶ Retaining the copyright to your article

Submit your next manuscript at ▶ editor.ijaamm@gmail.com